ARTICLE

FTIR Spectroscopic Study of Thioanisole and its Two Halogenated Derivatives†

Jiaqi Xin[a], Jianzhi Xu[a], Ya-Ke Li[a], Jianbao Zhao[b], Brant E. Billinghurst[b], Hong Gao[c], Ziqiu Chen[d], Gao-Lei Hou[a*]

a. MOE Key Laboratory for Non-Equilibrium Synthesis and Modulation of Condensed Matter, School of Physics, Xi'an Jiaotong University, Xi'an 710049, China
b. Canadian Light Source Far-Infrared Beamline, Saskatoon S7N 2V3, Canada
c. Beijing National Laboratory for Molecular Sciences (BNLMS), Institute of Chemistry, Chinese Academy of Sciences, Beijing 100190, China
d. College of Chemistry and Chemical Engineering, Lanzhou University, Lanzhou 730000, China

(Dated: Received on May 12, 2025; Accepted on September 8, 2025)

The rovibrational spectra of thioanisole (TA) and its halogenated derivatives, 3-fluorothioanisole (3FTA) and 3-chlorothioanisole (3ClTA), were measured using synchrotron-based Fourier transform infrared spectroscopy (FTIR) at the Canadian Light Source. Combined with density functional theory calculations, the stable structures and vibrational modes of TA, 3FTA, and 3ClTA in their vibrational states were analyzed. The theoretical vibrational mode frequencies were corrected by simulating the rotational structure of a vibrational band. The contributions of the *cis*- and *trans*-isomers of 3FTA and 3ClTA to the FTIR spectra at 298 K were estimated using the Boltzmann distribution, revealing their coexistence in the experimental spectra. The results indicate that both fluorine and chlorine substitution significantly affect the vibrational modes, particularly in the benzene ring. Compared to TA, the FTIR spectra of 3FTA and 3ClTA show changes in the frequencies and intensities of some vibrational modes, with halogen substitution causing specific modes to shift to higher wavenumbers. A comparison of the FTIR spectra of TA, 3FTA, and 3ClTA highlights the influence of halogen substitution on vibrational properties, emphasizing how the type and position of the substituent affect frequency shifts and spectral intensities. These findings provide deeper insights into how halogenation alters vibrational spectra, which is crucial for further spectral analysis and molecular structure determination.

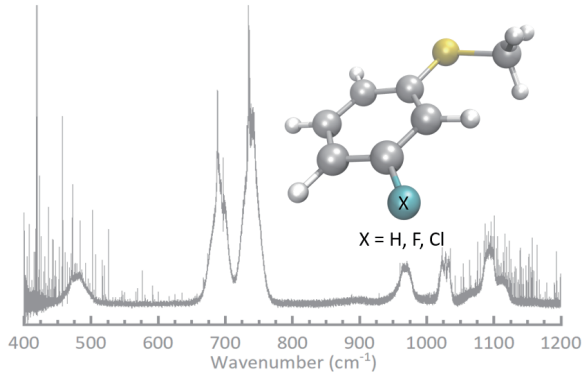

Key words: Fourier transform infrared spectroscopy, Thioanisole, Halogenated derivatives

I. INTRODUCTION

Thioanisole (TA) is a fundamental benzene derivative consisting of a benzene ring and a methylthio group (-SCH_3). TA has a wide range of applications in industrial and practical contexts. For example, in the pharmaceutical industry, it is used as a raw material for the synthesis of antibiotics and anti-ulcer drugs, and is a routinely utilized scavenger in peptide synthesis [1, 2]. In the pesticide industry, it is employed in the synthesis of insecticides, fungicides, and herbicides [3]. It is also used as an additive in lubricants and as a raw materi-

† Part of Special Issue dedicated to Professor Fanao Kong on the occasion of his 90th birthday.

* Author to whom correspondence should be addressed.
E-mail: gaolei.hou@xjtu.edu.cn

al for fragrance synthesis [4, 5]. However, regarding the stable molecular structures of TA across different states, it remains a topic of debate, and interpretations of spectroscopic findings have not yet been fully resolved.

Currently, it has been confirmed that the TA molecule adopts a planar structure in its electronic ground state (S_0), first excited state (S_1), and cationic ground state (D_0). This conclusion is supported by multiple theoretical calculations and experimental studies. As early as in 1987, Schaefer and co-workers inferred through nuclear magnetic resonance analysis that the most stable structure of TA in solution is planar [6–8]. Subsequent studies based on gas electron diffraction spectroscopy [9], laser-induced fluorescence and dispersed fluorescence spectroscopy [10], as well as zero kinetic energy photoelectron spectroscopy [11], concluded that the TA molecule adopts only a single stable planar conformer. The rotational constants derived from free-jet microwave spectroscopy clearly indicate the presence of a planar conformer, with no transitions observed corresponding to a perpendicular conformer [12]. Nevertheless, certain exceptions have been noted. Zaripov *et al.*, based on electron diffraction spectroscopy, proposed that the stable molecular configuration of TA is neither planar nor perpendicular [13]. Instead, they observed a twisted structure, with a dihedral angle of approximately 45° between the benzene ring and the methylthio group. Moreover, previous studies utilizing ultraviolet photoelectron and Raman spectroscopy suggested that both planar and perpendicular conformers could coexist in the S_0 state [14, 15].

The stable conformers of TA derivatives are also under discussion. Due to the strong conjugative interaction between the benzene ring and the substituent functional groups, the stable configurations of most phenyl ether derivatives have been found to be planar [16–19]. For instance, 4-chloro-3-fluoroanisole [20] and 3-chloro-*N*-methylaniline [21] have been confirmed as stable planar conformers in the S_0, S_1, and D_0 states, as determined by resonance-enhanced two-photon ionization (RE2PI) and mass-analyzed threshold ionization (MATI). Other molecules, including *m*-fluoroanisole [22], *m*-chloroanisole [23], and *m*-methoxystyrene [24], similarly exhibit planar structures. Nevertheless, a few stable non-planar conformers have also been documented, as observed in $C_6H_5SCF_3$ [25–27] and *N*-methylaniline derivatives [28–30]. For phenyl derivative molecules, the number, type (intrinsic properties), and relative positions of substituents can exert varying degrees of influence on the physicochemical properties of the molecule, with the influence extent not necessarily being the same across different states. Spectroscopic analyses, including Fourier transform infrared spectroscopy (FTIR) and two-color resonant two-photon mass-analyzed threshold ionization spectroscopy, revealed that *trans*-2-fluoroanisole adopts a non-planar stable structure in its S_0 state [31, 32]. In contrast, the *cis*-planar isomer of 3-fluoroanisole was found to be the most stable [22], due to the weaker substituent effect between the fluorine atom and the -OCH_3 group in the meta-position. In *trans*-2-fluoroanisole, however, the stronger substituent effects (both steric and inductive effects) caused by the fluorine atom in the ortho-position play a significant role.

Recently, Zhang *et al.* investigated the *cis*- and *trans*-3-chlorothioanisole and 3-fluorothioanisole using RE2PI, MATI spectroscopy, and quantum chemical calculations [33, 34]. They determined the first electronic excitation energies and adiabatic ionization energies, and also obtained the vibrational spectra in the S_1 and D_0 states. By comparing the two derivatives of TA, they found that the inductive effects of the substituents are qualitatively correlated with the energy changes relative to the unsubstituted molecule. These studies have contributed to further research on TA and its derivatives, but the vibrational spectral data for the neutral ground state of TA and derivatives is still missing.

In this work, we employed FTIR spectroscopy based on synchrotron radiation to acquire high-resolution infrared spectral data for TA and its derivatives substituted with halogen elements (F and Cl). With density functional theory (DFT) calculations, we identified the vibrational transitions from the ground state to the first excited state for certain vibrational modes of TA, 3-fluorothioanisole (3FTA), and 3-chlorothioanisole (3ClTA) and determined the stable structure of TA and its derivatives in the S_0 state and conducted a detailed analysis of their vibrational modes. Subsequently, we compared the experimental spectra of the three molecules to investigate the effect of substituents, and interesting changes in the vibrational modes of TA upon substitution with F and Cl have been observed and explained.

II. EXPERIMENTAL METHODS

The rovibrational spectra of TA, 3FTA, and 3ClTA

DOI: 10.1063/1674-0068/cjcp2505061

were measured utilizing high resolution FTIR spectrometer equipped with synchrotron source at the Canadian Light Source. In terms of signal-to-noise ratios, the use of synchrotron radiation offers an advantage of up to an order of magnitude over conventional thermal light sources [35, 36]. Spectra were collected at a series of pressures at room temperature because spectra at multiple pressures are needed for bands with substantial intensity differences in the same spectral window. Spectra of TA in the range from 400 to 1300 cm^{-1} were collected at 0.0274 Torr using a Ge:Cu detector and KBr beamsplitter. Spectra of 3FTA in the range from 30 to 600 cm^{-1} were collected at 0.3244 Torr using a QMC Instruments Superconducting Niobium TES Bolometer detector and 6 micron Mylar (T222) beamsplitter. Spectra of 3FTA in the range from 400 cm^{-1} to 1300 cm^{-1} were collected at 0.013 Torr using a Ge:Cu detector and KBr beamsplitter. Spectra of 3ClTA in the range from 400 cm^{-1} to 1300 cm^{-1} were collected at 0.027 Torr using a Ge:Cu detector and KBr beamsplitter. The sample was introduced into the 2 m multipass cell with an absorption path length of 72 m and low resolution spectra were recorded to optimize the pressure before the high resolution scans started. Once a sufficient signal-to-noise ratio was achieved, the sample compartment was evacuated and background spectrum was recorded. Ultimately, the interferograms were processed to obtain spectra using the OPUS software package provided by Bruker.

III. COMPUTATIONAL METHODS

The geometry optimization and infrared spectra calculations for TA and its halogenated derivatives were performed using the Gaussian 16 program [37]. We optimized the geometries at the B3LYP/cc-pVTZ level of theory, and the resulting structures are shown in FIG. 1. To accurately simulate vibrational spectra in terms of both frequency and intensity, it is necessary to account for mechanical and electrical anharmonicity. For very small molecules, rovibrational energy levels can be computed via full variational methods [38]; however, for larger systems, simplified and more computationally affordable approaches based on either variational [39] or perturbational [40] strategies are required. Among these, second-order vibrational perturbation theory (VPT2) offers an effective and computationally efficient framework [41]. Therefore, this study employed the VPT2 method to calculate vibrational energy levels, transition intensities, and rotational constants, including fundamentals, overtones, and combination bands. These calculations were also performed at the B3LYP/cc-pVTZ level, as the B3LYP functional has been demonstrated to be a highly suitable choice for anharmonic frequency calculations [42]. To validate our choice of functional, we also performed anharmonic calculations using ωB97X-D and M06-2X. These functionals produced results that were in worse agreement with the experiment compared to B3LYP, showing B3LYP to be the more suitable choice in this study. More detailed results are available in Supplementary materials (SM). All calculated stick spectra were convolved using a Gaussian function with an 8 cm^{-1} FWHM, and the resulting anharmonic vibrational spectra were plotted using the Multiwfn program [43]. Subsequently, the rotational constants obtained from the Gaussian output were used as input for the Pgopher software [44] to simulate the fundamental band transition spectra for these molecules.

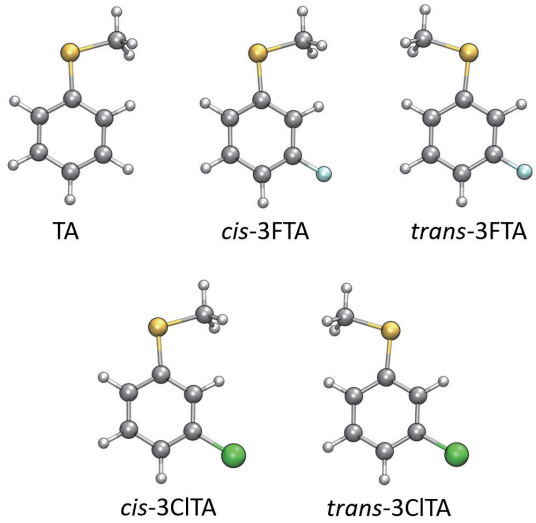

FIG. 1 Chemical structures of thioanisole (TA) and its two halogenated derivatives. Yellow spheres represent the sulfur (S) atom, blue spheres represent the fluorine (F) atom, and green spheres represent the chlorine (Cl) atom.

The spectrum of TA in the 400–700 cm^{-1} region is shown in FIG. 2. The upper trace shows the "raw spectrum", which includes sharp features due to H_2O, D_2O, and HDO lines from the samples of the preceding beamline users. These are readily discerned from the broader TA features. The lower trace shows the lines arising from H_2O, D_2O, and HDO from the HITRAN database. It is evident from the comparison in FIG. 2 that the sharp lines in the experimental spectrum indeed origi-

DOI: 10.1063/1674-0068/cjcp2505061

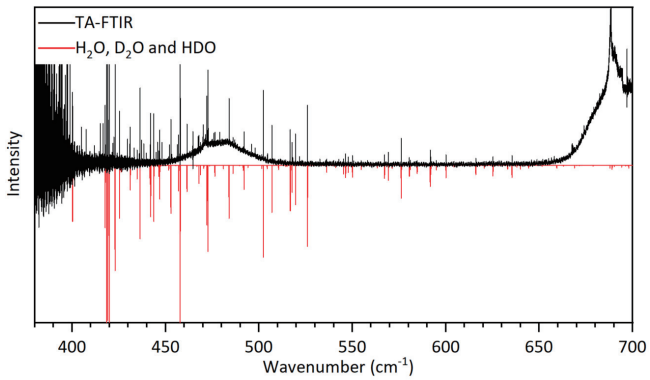

FIG. 2 An overview of the infrared spectrum of TA. The upper black trace shows the raw experimental spectrum, which includes multiple lines due to H_2O, D_2O, and HDO impurities. The lower red trace shows the lines arising from H_2O, D_2O, and HDO transitions reported in the HITRAN database.

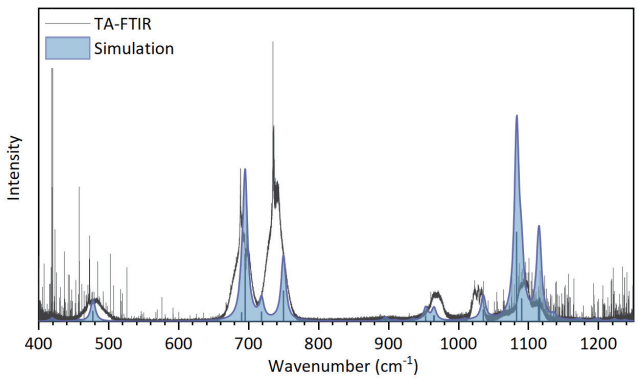

FIG. 3 FTIR spectrum (black) and simulated IR spectrum of TA. The B3LYP/cc-pVTZ computed spectrum (blue sticks) is convolved with an 8 cm^{-1} FWHM Gaussian function (blue shaded area). The FTIR spectrum of TA was recorded in the 400–1250 cm^{-1} range at a resolution of 0.000960 cm^{-1}. The spectrum was acquired at a pressure of 0.0274 Torr, a temperature of 294.05 K, and with a 72 m absorption pathlength.

nate from the H_2O, D_2O, and HDO. More details regarding the spectra of TA, 3FTA, and 3ClTA are presented in SM.

IV. RESULTS AND DISCUSSION

The FTIR spectrum of TA in 400–1300 cm^{-1} is presented as the black trace in FIG. 3, shown together with the FTIR spectrum is the B3LYP/cc-pVTZ computed vibrational spectrum of TA depicted by the blue vertical lines and the convolution in blue. The overall shape of the calculated spectrum matches well with the experimental spectrum in terms of the frequency positions of the peaks, but the relative intensities of some peaks show slight differences. This effect is possibly due to the flaws of DFT in calculating infrared spectra [45].

A. FTIR spectrum of thioanisole

Considering the controversy regarding the two molecular conformations of thioanisole, the planar and perpendicular conformations were subjected to optimization using B3LYP/cc-pVTZ. It was found that the perpendicular conformation converted into the planar one after optimization, indicating that the planar conformation is the stable conformation of TA in the S_0 state (Cartesian coordinates of TA are provided in SM). This result is consistent with the findings of most studies mentioned in the introduction.

Seven broad features at 479, 688, 735, 968, 1028, 1094, and 1112 cm^{-1} can be observed in the FTIR spectrum of TA. The two peaks in the range of 650–800 cm^{-1} are the broadest and most intense features. Computational analysis (see Table I for details of the computed modes) indicates that the most intense feature originates mainly from two modes, which primarily consist of out-of-plane C–H bending, corresponding to frequencies at 695 and 750 cm^{-1}. The anharmonic mode at 477 cm^{-1} matches quite well with the experimental spectrum and originates from CCC twisting. The FTIR features in the 650–800 cm^{-1} range and at 1035 cm^{-1} exhibit a slight red shift compared to the calculated anharmonic vibrational modes. The calculated spectrum reveals three peaks in the 650–800 cm^{-1} range, which are comprised of three anharmonic modes at 690, 695, 718, and 750 cm^{-1}. These calculated modes primarily involve ring torsion and out-of-plane C–H bending on the benzene ring, along with in-plane C–S and S–CH_3 stretching vibrations. The peak at 1035 cm^{-1} predominantly arises from in-plane C–H bending and C–C stretching on the benzene ring. It is important to note that in the FTIR experimental spectrum, two peaks with significant intensity are observed in the 650–800 cm^{-1} range. This may be attributed to the blending of certain features in the observed spectrum. The FTIR feature at 968 cm^{-1} appears to consist mainly of two modes calculated at 953 and 965 cm^{-1}, although this feature is slightly blue-shifted relative to the calculated 953 cm^{-1} vibration. The first calculated mode originates from out-of-plane C–H bending of the CH_3 group, while the second arises from in-plane C–H bending of the CH_3 group. The calculated anharmonic modes in the 1040–1140 cm^{-1} range match the experi-

DOI: 10.1063/1674-0068/cjcp2505061

TABLE I Experimental and B3LYP/cc-pVTZ calculated vibrational frequencies, intensities and vibrational assignments of TA. Frequencies are given in cm^{-1} and intensities are in km/mol.

Band	Assignment	Caculated results		Experimental results	
		Frequency	Intensity	Frequency	Intensity
ν_8	CCC twisting	477.47	7.11	479.01	0.15
ν_{10}	sym. stretch C-S-C	690.14	6.22	686.00	0.51
ν_{11}	ring torsion	694.96	46.84	690.51	0.71
ν_{12}	asym. stretch C-S-C	718.24	6.67	730.00	0.59
ν_{13}	C-H bend	749.74	21.27	738.31	1.01
ν_{16}	CH_3 wag	953.10	3.82	965.63	0.21
ν_{18}	CH_3 rock	964.89	4.01	968.49	0.18
ν_{21}	sym. stretch CC	1035.36	7.99	1028.18	0.25
ν_{22}	sym. stretch CC	1083.11	62.68	1093.28	0.27
ν_{23}	CC stretch/CH bend	1089.91	15.95	1094.40	0.29
$\nu_6+\nu_{11}$		1114.22	14.21	1110.22	0.12
$\nu_7+\nu_{10}$		1115.60	16.46	1112.60	0.13

mental spectrum well in terms of frequency positions.

In order to more accurately determine the frequency positions of the vibrational modes, we simulated the rovibrational spectra of different vibrational modes transitioning from the ground state to the excited state. Taking the feature at 1028 cm^{-1} as an example (see FIG. 4), we used the Pgopher to simulate the rovibrational band of the most intense vibrational mode in this region, ν_{21}. The simulation results show that the rovibrational band of vibrational mode closely matches the FTIR experimental spectrum. By comparing the simulated rovibrational spectra with the experimental data, we corrected the theoretical vibrational mode frequencies, thereby obtaining more accurate vibrational mode positions. The final band origins of the experimental vibrational modes, refined using our rovibrational spectral simulations, are presented in Table I. Additional simulations for other vibrational bands of TA are provided in SM. Simultaneously, the calculated and experimental results for TA were compared with existing vibrational assignments from the literature [46, 47] (see SM for the comparison), which confirms the reliability of our calculations. Furthermore, regarding the periodic "fringe" structures in the FTIR spectrum, similar to those in FIG. 4 and FIG. S10 (SM), it should be clarified that these are not real rotational information. They are experimental artifacts caused by vibrations from the vacuum pump and have no physical significance.

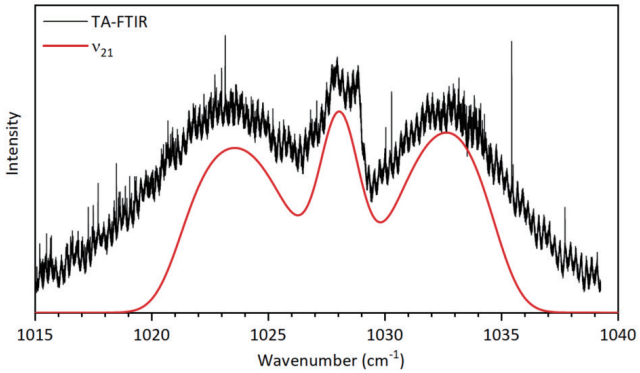

FIG. 4 FTIR (black) and simulated rovibrational (red) spectra of TA at 1028 cm^{-1}. The simulated spectrum was convolved using a Gaussian function with a 2 cm^{-1} FWHM.

B. FTIR spectrum of 3-fluorothioanisole

Similar to TA, before starting the spectral analysis, the planar and perpendicular conformations of 3FTA were optimized. The results show that the stable conformation of 3FTA in the S_0 state is the planar conformation. As shown in FIG. 1, the planar structure of 3FTA has two isomers: *cis*- and *trans*-3FTA. At the B3LYP/cc-pVTZ level, we optimized the geometric structures of the two isomers and performed vibrational analysis to obtain the thermal corrections. Single-point energy calculations for both isomers were then carried out using the CCSD(T)/cc-pVTZ. By combining the single-point energies with the thermal corrections, the Gibbs free energies of the isomers were determined. The contribution of each isomer to the FTIR spectrum under thermal equilibrium was subsequently estimated using the Boltzmann distribution. The results show that at 298.15 K, the *cis*- and *trans*-isomers contribute 55.83% and 44.17%, respectively, suggesting

DOI: 10.1063/1674-0068/cjcp2505061

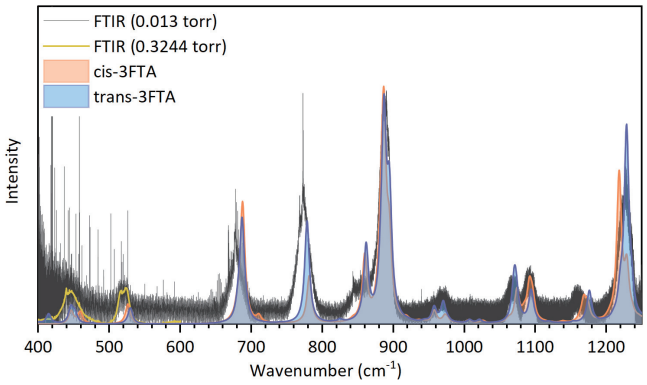

FIG. 5 FTIR spectra (black and yellow) and simulated infrared spectra (blue and orange curves) of 3FTA. The blue curve corresponds to the anharmonic infrared spectrum of the *trans*-3FTA, while the orange curve represents the anharmonic infrared spectrum of the *cis*-3FTA. The B3LYP/cc-pVTZ computed anharmonic spectrum (blue sticks) is convolved with an 8 cm^{-1} FWHM Gaussian function. The yellow trace shows the FTIR spectrum over the 400–600 cm^{-1} range, recorded at a resolution of 0.05 cm^{-1}, at a pressure of 0.3244 Torr, a temperature of 328.25 K, and with a 72 m absorption pathlength. The black trace shows the FTIR spectrum over the 400–1250 cm^{-1} range, recorded at a resolution of 0.00096 cm^{-1}, at a pressure of 0.013 Torr, a temperature of 295.55 K, and with a 72 m absorption pathlength.

that both isomers coexist and contribute to the FTIR spectrum. The calculated position and intensity of the *cis*- and *trans*-3FTA modes are listed in SM, with the *cis*-isomer highlighted in orange and the *trans*-isomer in blue in FIG. 5.

The FTIR spectrum reveals eleven distinct features at 445, 520, 677, 773, 854, 888, 970, 1068, 1092, 1161, and 1227 cm^{-1}. The most prominent features are observed in the 800–900 cm^{-1} range. According to anharmonic calculations, these features primarily arise from the fundamental peaks at 860, 883, 887 cm^{-1}, as well as the overtone peak at 895 cm^{-1}. The modes at 860 and 883 cm^{-1} are primarily due to the out-of-plane C–H bending of the benzene ring, while the 887 cm^{-1} feature originates from vibrations of the ring, including C–F stretching and C–S stretching. DFT calculations show that the feature at 445 cm^{-1} arises from CCC twist and in-plane C–F bending on the benzene ring, while the feature at 520 cm^{-1} corresponds to in-plane C–C bending. The 677 cm^{-1} peak is attributed to ring torsion and in-plane C–C bending on the ring, and the 773 cm^{-1} peak is caused by out-of-plane C–H bending of three adjacent hydrogens on the benzene ring. The feature at 970 cm^{-1} consists of vibrational modes at 958 and 972 cm^{-1} for *cis*-, 957 and 970 cm^{-1} for *trans*-, and out-of-plane C–H bending on the methyl group at 958 and 957 cm^{-1}, and the modes at 972 and 970 cm^{-1} associated with in-plane C–H bending on the methyl group. The feature at 1068 cm^{-1} is composed of in-plane C–H bending, C–C stretching, and C–S stretching. The feature at 1092 cm^{-1} is similar to that at 1068 cm^{-1} and involves the same three vibrational modes. The peak at 1161 cm^{-1} is attributed to in-plane C–H bending and S–CH_3 stretching, while the 1227 cm^{-1} feature primarily arises from C–C stretching, C–H bending, C–F stretching, and C–S stretching modes on the benzene ring.

C. FTIR spectrum of 3-chlorothioanisole

Similar to 3FTA, the planar and perpendicular conformations of 3ClTA were optimized. The results show that the conformation of 3ClTA in the S_0 state is planar. As shown in FIG. 1, two isomers of 3ClTA, *cis*-3ClTA and *trans*-3ClTA, were considered. The contributions of these two isomers to the FTIR at 298 K were estimated based on the Boltzmann distribution under the assumption of thermal equilibrium. The results indicate that the *cis*- and *trans*-isomers contribute 55.93% and 44.07%, respectively, suggesting that both isomers contribute to the FTIR spectrum and coexist in the experiment. The anharmonic calculated positions and intensities of the *cis*- and *trans*-3ClTA modes are listed in SM, with the *cis*-isomer highlighted in orange and the *trans*-isomer in blue in FIG. 6.

The FTIR spectrum exhibits several distinct features at 427, 677, 782, 867, 969, 997, 1086, and 1127 cm^{-1}. The most intense feature appears around 782 cm^{-1}, where the theoretical anharmonic IR spectrum indicates that the corresponding vibrational modes are mainly found at 776 and 779 cm^{-1} for *cis*- and 772 and 775 cm^{-1} for *trans*-3ClTA. The 772 and 779 cm^{-1} modes are attributed to out-of-plane C–H bending, while the 775 and 776 cm^{-1} peaks correspond to C–Cl stretching and C–S stretching. Additional theoretical calculations show that the 427 cm^{-1} mode is due to out-of-plane C–H bending and C–C bending on the benzene ring, while the mode at 677 cm^{-1} is primarily caused by ring torsion. The mode at 867 cm^{-1} mode is associated with out-of-plane C–H bending on the ring. The feature at 969 cm^{-1} arises from two modes at 958 and 970 cm^{-1}, where the former corresponds to out-of-plane C–H wagging on the methyl group, and the latter to in-plane C–H rocking. The vibrational mode at 997 cm^{-1} is due to CCC scissoring on the benzene ring.

DOI: 10.1063/1674-0068/cjcp2505061

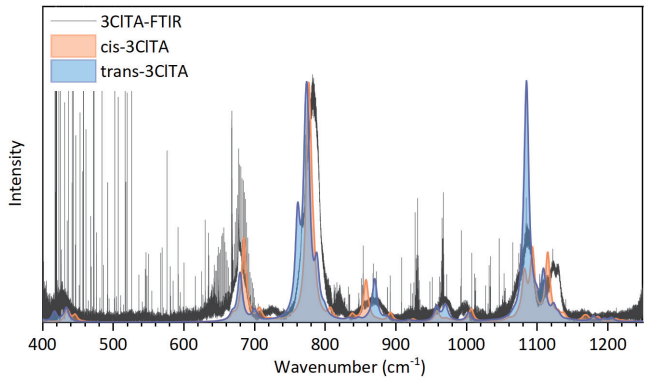

FIG. 6 FTIR spectra (black) and simulated infrared spectra (blue and orange curves) of 3ClTA. The blue curve corresponds to the anharmonic infrared spectrum of the *trans*-3ClTA, and the orange curve represents the anharmonic infrared spectrum of the *cis*-3ClTA. The B3LYP/cc-pVTZ computed anharmonic spectrum is convolved with an 8 cm^{-1} FWHM Gaussian function. The black trace shows the FTIR spectrum over the 400–1250 cm^{-1} range, recorded at a resolution of 0.00096 cm^{-1}, at a pressure of 0.027 Torr, a temperature of 294.85 K, and with a 72 m absorption pathlength.

The mode at 1086 cm^{-1} primarily involves C–Cl stretching, C–S stretching, C–C stretching, and in-plane C–H bending, with the same type of mode observed at 1127 cm^{-1}.

The calculated anharmonic spectra of *cis*- and *trans*-3ClTA are generally similar in terms of both wavelength positions and relative intensities. The experimental spectra and calculated results are consistent with previously reported frequencies [48] for *ortho*-substituted benzene rings, where the features are mainly attributed to out-of-plane aromatic C–H bending and ring skeleton vibrations.

D. FTIR spectra comparison of the TA, 3FTA, and 3ClTA

Substituents significantly affect the vibrational spectra of molecules through multiple mechanisms, such as electronic effects, symmetry changes, and vibrational mode coupling. The type, position, and electronic properties of the substituent all contribute to distinct alterations in the vibrational modes, which result in differences between the spectra of substituted and unsubstituted molecules. In the following, the FTIR spectra of TA and its derivatives, 3FTA and 3ClTA, are compared to investigate the effect of halogen substitution on the vibrational spectra (as shown in FIG. 7).

The introduction of a substituent leads to changes in both the number and position of spectral bands in the benzene ring. The structural modification caused by the

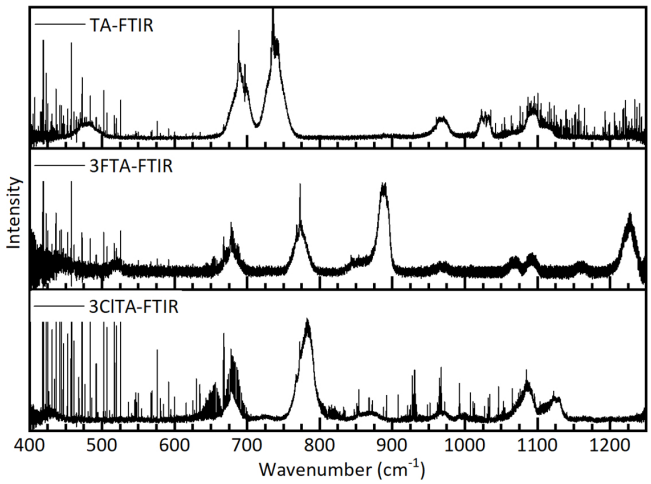

FIG. 7 FTIR spectra of TA, 3FTA, and 3ClTA.

substituent creates new vibrational modes, resulting in the appearance of additional bands in the spectrum. Anharmonic calculations show that when the hydrogen on the benzene ring of phenyl methyl sulfide is replaced by fluorine, a new in-plane C–F stretching vibration appears at 886 cm^{-1}. Similarly, when the hydrogen is replaced by chlorine, a C–Cl stretching vibration is observed at 775 cm^{-1}. For *cis*-3ClTA, a new out-of-plane C–H bending vibration mode of the benzene ring adjacent to the -SCH_3 group appears at 857 cm^{-1}. Previous studies on the spectrum of fluorobenzene [49] have also confirmed this phenomenon. The substitution of a fluorine atom reduces the symmetry of the benzene molecule, leading to a significant splitting of previously degenerate energy levels. Additionally, this substitution alters the electronic distribution within the fluorobenzene molecule, which in turn causes a frequency shift in the energy levels of the C–H stretching modes.

Furthermore, the electronic effects of the substituent modify the electron density distribution within the molecule, which in turn alters the electronic environment of the bonds. This leads to shifts in the frequencies of the vibrational modes and changes in the positions of the spectral bands. Comparing the key features in the FTIR spectra of the three molecules, the vibrational mode at 688 cm^{-1} in the TA spectrum corresponds to the ring torsion. In the spectrum of 3FTA, this vibrational mode is observed at 677 cm^{-1}, while in 3ClTA, it also appears at 677 cm^{-1}. This indicates that the frequency of this mode remains largely unchanged after halogen substitution. At 735 cm^{-1} in the TA spectrum, the vibrational mode is associated with the out-of-plane C–H bending on the benzene ring. In 3FTA, this

DOI: 10.1063/1674-0068/cjcp2505061

mode shifts to 773 cm^{-1}, and in 3ClTA, it is observed at 785 cm^{-1}, indicating a significant shift to higher wavenumber upon halogen substitution. The vibrational mode at 966 cm^{-1} in the TA spectrum is attributed to the out-of-plane wagging of C–H in the methyl group. In the spectra of 3FTA and 3ClTA, this mode is observed at 957 cm^{-1} and 956 cm^{-1}, respectively, indicating minimal changes in frequency relative to TA. Similarly, the mode at 971 cm^{-1} in the TA spectrum, corresponding to the in-plane rocking of C–H in the methyl group, is observed at 970 cm^{-1} for 3FTA and 969 cm^{-1} for 3ClTA, showing no significant shifts in frequency position. The vibrational mode at 1028 cm^{-1} in the TA spectrum, assigned to the C–C skeletal stretching in benzene ring, shifts to 1089 cm^{-1} in 3FTA and 1073 cm^{-1} in 3ClTA, indicating a noticeable shift to higher wavenumbers. Additionally, the mode at 1095 cm^{-1} in the TA spectrum, corresponding to the stretching of the carbon atom bonded to the -SCH_3 group along with some in-plane C–H bending, is observed at 1089 cm^{-1} in 3FTA and 1086 cm^{-1} in 3ClTA, showing minimal variation in frequency compared to TA.

The spectral analysis reveals that the majority of vibrational modes in the TA spectrum remain unchanged in 3FTA and 3ClTA after substitution of H atoms on the benzene ring with F and Cl atoms. Only a small subset of vibrational modes exhibits frequency shifts, particularly those associated with the presence of Cl/F atoms. The vibrational features related to Cl/F atoms are observed to shift to higher wavenumbers in the 3FTA and 3ClTA spectra, compared to the TA spectrum. The effect of halogens on the stretching vibrations of the benzene ring is primarily manifested in their inductive effect on the ring. The high electronegativity of the halogen causes a strong electron withdrawal from the benzene ring, leading to a polarization of the electron density on the ring. This increases the bond force constant of the C–C bonds in the benzene ring, causing the absorption peak frequency to shift to higher wavenumbers. Changes in vibrational modes after halogen substitution are commonly observed in benzene derivatives. Infrared and Raman spectroscopic studies of fluorobenzene, chlorobenzene, bromobenzene, and iodobenzene at room temperature [50] have shown clear shifts in the characteristic peaks of substituent-related vibrational modes. Specifically, the vibrational characteristic peaks of halogenated benzenes exhibit a blue shift as the atomic mass of the halogen decreases. This effect occurs because heavier halogens have lower electronegativity, which weakens their inductive effect. As a result, the force constant of the C–C bonds in the benzene ring decreases, leading to a shift of vibrational frequencies to lower wavenumbers.

Substituents also exert a significant influence on the intensities of various vibrational modes within a molecule. Depending on the nature of the substituent, certain vibrational modes may be either enhanced or attenuated, resulting in a shift in the relative intensities of the corresponding spectral bands. This phenomenon arises from the interaction between the substituent and the benzene ring, which modifies the molecular dipole moment and consequently affects the infrared activity and intensity of specific vibrational modes. In the FTIR spectrum of 3FTA, the most prominent intensity is observed near 890 cm^{-1}, predominantly arising from the C–C stretching and C–F stretching vibrations. In contrast, the FTIR spectrum of 3ClTA exhibits the highest relative intensity around 780 cm^{-1}, primarily due to the contributions of C–C in-plane bending and C–Cl stretching vibrations. For TA, the highest intensity is observed near 730 cm^{-1}, which is mainly attributed to out-of-plane C–H bending vibrations. The substantial electronegativity of halogen atoms induces a pronounced electron-withdrawing effect on the benzene ring, resulting in a redistribution of the electron density. This alters the instantaneous dipole moment associated with the skeletal vibrations, which leads to changes in the relative intensities of the spectral features.

V. CONCLUSION

The FTIR spectra of TA, 3FTA, and 3ClTA have been reported for the first time. Spectroscopic and calculated results indicate that both *cis*- and *trans*-isomers of 3FTA and 3ClTA coexist in the S_0 states, adopting planar structures with C_s symmetry. By employing anharmonic calculations combined with simulated rovibrational spectra for different vibrational modes, the spectral features of TA and its two derivatives were assigned to specific vibrational modes, including fundamental, overtone, and combination band transitions. A comparative analysis of the infrared spectra of TA, 3FTA, and 3ClTA reveals that halogen substitution on the benzene ring of TA significantly influences the spectral characteristics. The substitution in-

DOI: 10.1063/1674-0068/cjcp2505061

troduces new vibrational modes such as C–F and C–Cl stretching vibrations and induces frequency shifts in specific modes. The strong electronegativity of halogens generates an inductive effect, which increases the force constants of C–C bonds within the benzene ring, resulting in a shift of the associated vibrational features toward higher wavenumbers. Furthermore, the introduction of substituents alters the molecular dipole moment, leading to observable changes in the intensity of vibrational modes. This study provides comprehensive spectral characterization, elucidates the role of halogen substitution, and enhances the understanding of vibrational spectra in TA and its derivatives. Future investigations may focus on refining theoretical methodologies for higher-precision spectral predictions and exploring the impact of substituents on other spectroscopic properties.

Supplementary materials: Comparisons of FTIR spectra with H_2O, D_2O, and HDO lines; simulated rotational spectra of TA, 3FTA, and 3ClTA; comparison of anharmonic vibrational spectra calculated with different functionals; detailed vibrational assignments; Cartesian coordinates.

VI. NOTES

There are no conflicts of interest to declare.

VII. ACKNOWLEDGEMENTS

This work was supported by the National Natural Science Foundation of China (No.223B2306), the Innovation Capability Support Program of Shaanxi Province (2023-CX-TD-49), and the Natural Science Basic Research Program of Shaanxi Province (2025JC-JCQN-043). The experimental work of this research was performed at the Canadian Light Source, a national research facility of the University of Saskatchewan.

[1] S. Charpentier, M. Amiche, J. Mester, V. Vouille, J. P. Le Caer, P. Nicolas, and A. Delfour, J. Biol. Chem. **273**, 14690 (1998).
[2] Y. Yang, *Peptide Global Ddeprotection/Scavenger-induced Side Reactions*, Oxford, UK: Academic Press, vol.3 43 (2016).
[3] Q. Gan and U. Jans, J. Agric. Food Chem. **54**, 7753 (2006).
[4] D. Heenan, K. Januszkiewicz, and H. Sulek, Wear **123**, 257 (1988).
[5] K. A. Günay, D. Benczédi, A. Herrmann, and H. A. Klok, Adv. Funct. Mater. **27**, 1603843 (2017).
[6] T. Schaefer and J. D. Baleja, Can. J. Chem. **64**, 1326 (1986).
[7] T. Schaefer and G. H. Penner, Can. J. Chem. **66**, 1641 (1988).
[8] T. Schaefer and G. H. Penner, Can. J. Chem. **66**, 1229 (1988).
[9] I. F. Shishkov, L. V. Khristenko, N. M. Karasev, L. V. Vilkov, and H. Oberhammer, J. Mol. Struct. **873**, 137 (2008).
[10] M. Nagasaka-Hoshino, T. Isozaki, T. Suzuki, T. Ichimura, and S. Kawauchi, Chem. Phys. Lett. **457**, 58 (2008).
[11] T. Vondrák, S. I. Sato, V. Špirko, and K. Kimura, J. Phys. Chem. A **101**, 8631 (1997).
[12] B. Velino, S. Melandri, W. Caminati, and P. Favero, Gazz. Chim. Ital. **125**, 373 (1995).
[13] N. Zaripov, J. Struct. Chem. **17**, 640 (1977).
[14] M. Dal Colle, G. Distefano, D. Jones, and A. Modelli, J. Phys. Chem. A **104**, 8227 (2000).
[15] Y. Yamakita, Y. Isogai, and K. Ohno, J. Chem. Phys. **124**, 104301 (2006).
[16] D. Xiao, D. Yu, X. Xu, Z. Yu, Y. Du, Z. Gao, Q. Zhu, and C. Zhang, J. Mol. Struct. **882**, 56 (2008).
[17] H. C. Huang, B. Y. Jin, and W. B. Tzeng, J. Photochem. Photobiol. A **243**, 73 (2012).
[18] K. S. Shiung, D. Yu, S. Y. Tzeng, and W. B. Tzeng, Chem. Phys. Lett. **524**, 38 (2012).
[19] L. Zhang, C. Dong, M. Cheng, L. Hu, Y. Du, Q. Zhu, and C. Zhang, Spectrochim. Acta A **96**, 578 (2012).
[20] S. Liu, W. Dai, D. Lin, M. Cheng, Y. Du, and Q. Zhu, J. Mol. Spectrosc. **338**, 15 (2017).
[21] S. Liu, L. Zhang, W. Dai, M. Cheng, Y. Du, and Q. Zhu, J. Mol. Spectrosc. **336**, 12 (2017).
[22] K. S. Shiung, D. Yu, H. C. Huang, and W. B. Tzeng, J. Mol. Spectrosc. **274**, 43 (2012).
[23] H. C. Huang, K. S. Shiung, B. Y. Jin, and W. B. Tzeng, Chem. Phys. **425**, 114 (2013).
[24] Y. Xu, S. Y. Tzeng, V. Shivatare, K. Takahashi, B. Zhang, and W. B. Tzeng, J. Chem. Phys. **142**, 124314 (2015).
[25] I. F. Shishkov, L. V. Khristenko, A. N. Rykov, L. V. Vilkov, N. I. Giricheva, S. A. Shlykov, G. V. Girichev, and H. Oberhammer, J. Mol. Struct. **876**, 147 (2008).
[26] S. Y. Kim, J. Lee, S. K. Kim, and Y. S. Choi, J. Phys. Chem. A **659**, 43 (2016).
[27] Y. Jin, J. Wang, Q. Gou, Z. Xia, and G. Feng, J. Mol. Struct. **1156**, 230 (2018).
[28] L. Zhang, S. Liu, C. Dong, M. Cheng, Y. Du, Q. Zhu, and C. Zhang, J. Mol. Spectrosc. **296**, 28 (2014).
[29] L. Zhang, S. Liu, M. Cheng, Y. Du, and Q. Zhu, J. Phys. Chem. A **120**, 81 (2016).

DOI: 10.1063/1674-0068/cjcp2505061

[30] S. Liu, W. Dai, L. Zhang, M. Cheng, Y. Du, and Q. Zhu, J. Mol. Struct. **1146**, 138 (2017).
[31] T. Isozaki, K. Sakeda, T. Suzuki, T. Ichimura, K. Tsuji, and K. Shibuya, Chem. Phys. Lett. **409**, 93 (2005).
[32] T. Isozaki, K. Sakeda, T. Suzuki, and T. Ichimura, J. Chem. Phys. **132**, 214308 (2010).
[33] Z. Zhang, Y. Du, G. L. Hou, and H. Gao, ACS Omega **7**, 8456 (2022).
[34] Z. Zhang, M. Li, G. L. Hou, and H. Gao, J. Phys. Chem. A **126**, 2541 (2022).
[35] A. McKellar, J. Mol. Spectrosc. **262**, 1 (2010).
[36] S. Albert, K. K. Albert, P. Lerch, and M. Quack, Faraday Discuss. **150**, 71 (2011).
[37] M. J. Frisch, G. W. Trucks, H. B. Schlegel, G. E. Scuseria, M. A. Robb, J. R. Cheeseman, G. Scalmani, V. Barone, G. A. Petersson, H. Nakatsuji, X. Li, M. Caricato, A. V. Marenich, J. Bloino, B. G. Janesko, R. Gomperts, B. Mennucci, H. P. Hratchian, J. V. Ortiz, A. F. Izmaylov, J. L. Sonnenberg, D. Williams-Young, F. Ding, F. Lipparini, F. Egidi, J. Goings, B. Peng, A. Petrone, T. Henderson, D. Ranasinghe, V. G. Zakrzewski, J. Gao, N. Rega, G. Zheng, W. Liang, M. Hada, M. Ehara, K. Toyota, R. Fukuda, J. Hasegawa, M. Ishida, T. Nakajima, Y. Honda, O. Kitao, H. Nakai, T. Vreven, K. Throssell, J. A. Montgomery, Jr., J. E. Peralta, F. Ogliaro, M. J. Bearpark, J. J. Heyd, E. N. Brothers, K. N. Kudin, V. N. Staroverov, T. A. Keith, R. Kobayashi, J. Normand, K. Raghavachari, A. P. Rendell, J. C. Burant, S. S. Iyengar, J. Tomasi, M. Cossi, J. M. Millam, M. Klene, C. Adamo, R. Cammi, J. W. Ochterski, R. L. Martin, K. Morokuma, O. Farkas, J. B. Foresman, and D. J. Fox, *Gaussian 16, Revision C.01*, Wallingford CT: Gaussian, Inc., (2019).
[38] A. G. Csaszar, C. Fabri, T. Szidarovszky, E. Matyus, T. Furtenbacher, and G. Czako, Phys. Chem. Chem. Phys. **14**, 1085 (2012).
[39] T. K. Roy and R. B. Gerber, Phys. Chem. Chem. Phys. **15**, 9468 (2013).
[40] M. Ringholm, D. Jonsson, R. Bast, B. Gao, A. J. Thorvaldsen, U. Ekström, T. Helgaker, and K. Ruud, J. Chem. Phys. **140**, 034103 (2014).
[41] J. Bloino, A. Baiardi, and M. Biczysko, Int. J. Quantum Chem. **116**, 1543 (2016).
[42] M. K. Kesharwani, B. Brauer, and J. M. Martin, J. Phys. Chem. A **119**, 1701 (2015).
[43] T. Lu and F. Chen, J. Comput. Chem. **33**, 580 (2012).
[44] C. M. Western, J. Quant. Spectrosc. Radiat. Transf. **186**, 221 (2017).
[45] V. Barone, M. Biczysko, and J. Bloino, Phys. Chem. Chem. Phys. **16**, 1759 (2014).
[46] C. Gellini, L. Moroni, and M. Muniz-Miranda, J. Phys. Chem. A **106**, 10999 (2002).
[47] M. X. Liu, B. B. Xie, M. J. Li, Y. Y. Zhao, K. M. Pei, H. G. Wang, and X. Zheng, J. Raman Spectrosc. **44**, 440 (2013).
[48] G. Varsányi, *Vibrational Spectra of Benzene Derivatives*, New York: Elsevier, (2012).
[49] M. Scotoni, S. Oss, L. Lubich, S. Furlani, and D. Bassi, J. Chem. Phys. **103**, 897 (1995).
[50] B. C. Pein, N. H. Seong, and D. D. Dlott, J. Phys. Chem. A **114**, 10500 (2010).

DOI: 10.1063/1674-0068/cjcp2505061